CHAPTER 6

Study of bubble visualization and dynamics

This chapter primarily focused on the visualization and analysis of pool boiling phenomena on hydrophilic and hydrophobic surfaces. Moreover, few of the bubble dynamics parameters have been estimated with the help of the semi analytical/an approximate models, due to limitation of the visualization resources.

6.1. Description of visualization procedure

A detailed explanation of the experimental apparatus and procedure has already been provided in Chapter 4. Boiling phenomena have been closely monitored by real-time temperature measurement data and the physical appearance of bubbles on the surface. Two glass windows were provided in the boiling chamber for visualization study. A standard operating procedure has been pre-set and followed during the bubble visualization in each case. The standard bubble visualization procedures are; -

- A Sony RX-100V camera has used for the bubble visualization. The maximum frame rate of the camera is 1000fps.
- Camera was mounted on a tripod and the height was adjusted in such a way that the camera should focus on the boiling surface.
- The camera was set at high-speed mode and the aperture focused on the boiling surface through a glass window, while an LED light source (SYSKA SS-LNTH 20111, 24W) was installed on the opposite side of the glass window for sufficient illumination.
- The video of bubbles (40X slow) was captured at 1000 fps for 20 second duration.

- The nucleate boiling phenomena were captured by the camera at various heat fluxes only when the system prevailed in a steady state condition.
- The high-speed video has been further converted into large number of images for bubble dynamics study.

6.2. Bubble growth and visualization

Nucleate boiling phenomenon was captured at various heat fluxes to analyse the nucleation sites and bubble growth mechanism on hydrophilic (Bare) and hydrophobic (coated) surfaces. Figure 6.1 depicts the snapshot of nucleate boiling phenomena at different heat fluxes of bare and coated surfaces (CS2-5). From Fig. 6.1, it is observed that as the supplied heat flux increases active nucleation sites also increase (Fig. 6.1e, f, & g) up the heat flux 206 kW/m^2, and then after bubbles start coalescing (Fig. 6.1d & h) with the surroundings bubbles and formed larger bubbles on the surface. The second observation is that on a hydrophilic (bare) surface (Fig 6.1 a, b, & c), the bubble size is relatively larger than the hydrophobic surface (Fig. 6.1 e, f, & h), because adhesion force is higher on a hydrophilic surface which requires higher buoyancy force to lift the bubble, resultant bubble growth is more and size is larger so that buoyancy force should overcome the adhesion force and detach from the surface.

Investigations have been also conducted on the shape of the bubbles, particularly as they approach the point of detachment. These studies have revealed that in a mature region of pool boiling, where individual bubbles merge to form larger entities, the bubble's shape at the brink of detachment varies and depending on whether the surface is hydrophobic or hydrophilic. Figures 6.2 and 6.3 capture the moments just before and after bubble detachment on both an uncoated and a coated (CS2-10) surface, respectively. On the bare (hydrophilic) surface bubbles maintain a nearly spherical shape, whereas on the coated (Hydrophobic) surface it exhibits a stretched form and makes a necking pattern prior to the detachment. During the detachment some portion of it remain on the surface which grow quickly and form another-

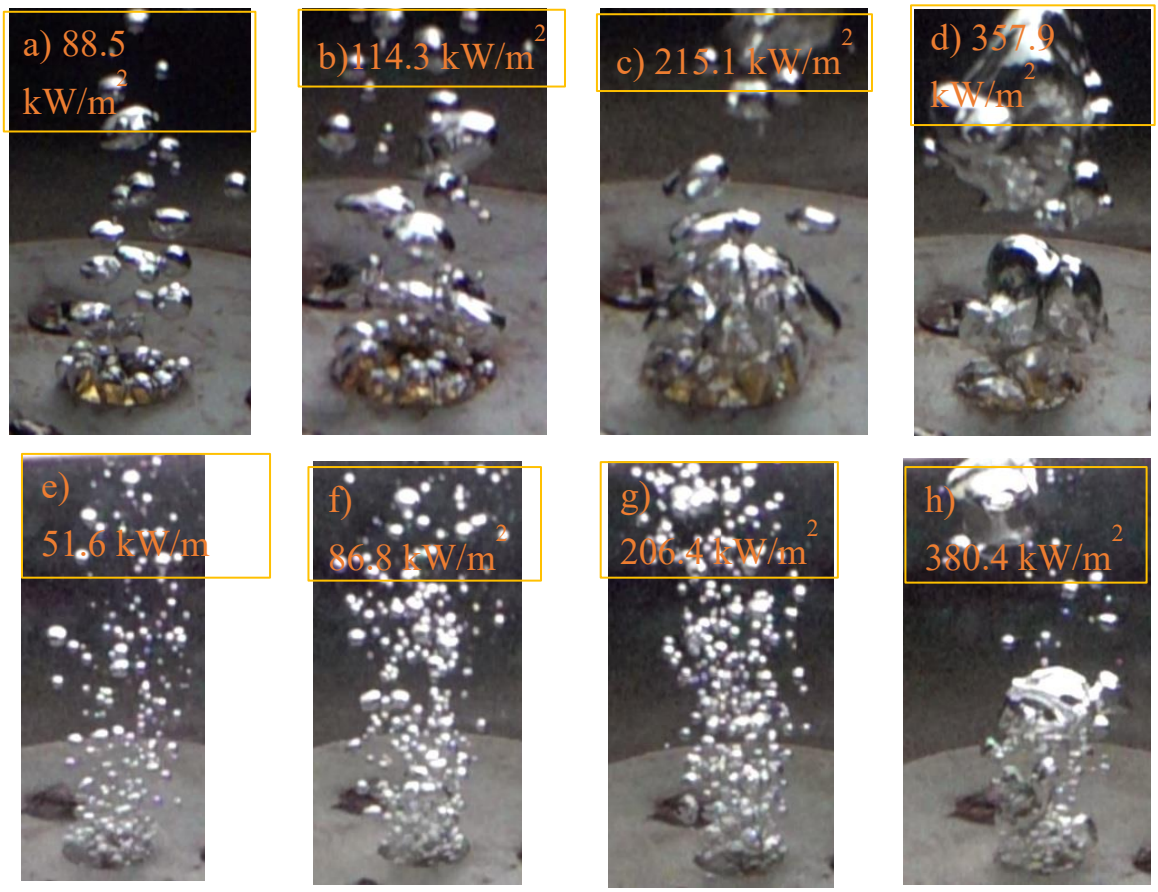

Fig. 6.1. Comparison of bubble generation (qualitative) on bare surface (hydrophilic) top row (a, b, c, & d), and composite surface CS2-5 (hydrophobic) bottom row (e, f, g, & h) at different heat flux.

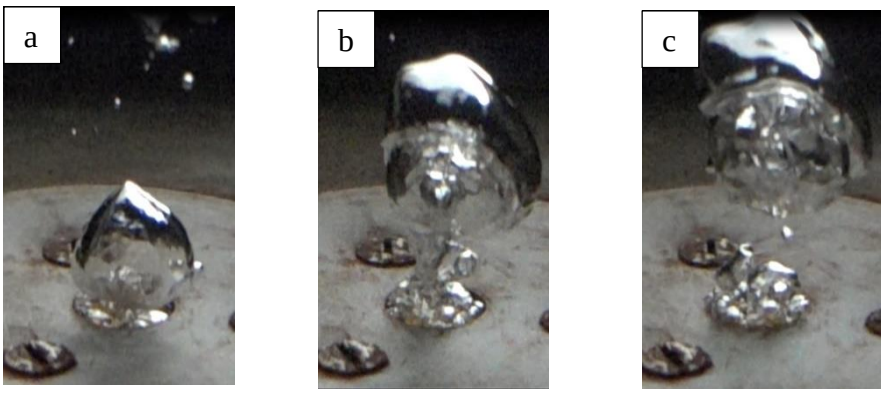

Fig. 6.2. Illustration of bubble formation and departure phenomena on bare (hydrophilic) surface (a) bubble formation (b) just before the departure (c) after the departure, in fully developed region of nucleate boiling.

bubble earlier than on a hydrophilic surface, resultant bubble waiting time reduced and departure frequency increased. A similar phenomenon was also observed by Jo et al. [132] in their experimental study.

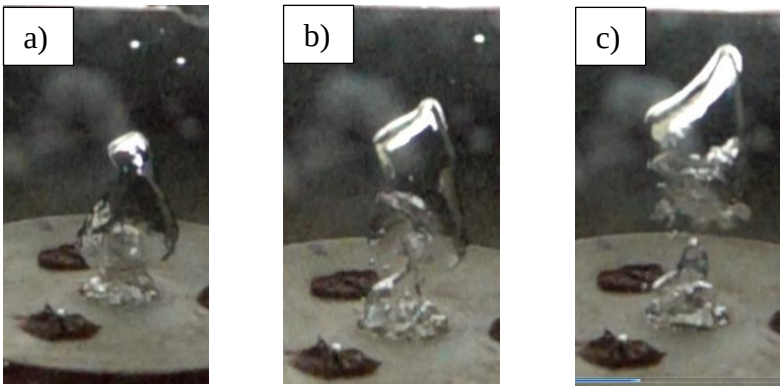

Fig. 6.3. Illustration of bubble formation and departure phenomena on coated (hydrophobic) surface CS2-10 (a) bubble formation (b) just before the departure (c) after the departure, in fully developed region of nucleate boiling.

6.3. Effect of surface roughness

It is well known that surface roughness and wettability are linked to each other and neither can be completely disregarded, therefore isolated effect of either of these two factors cannot be definitively claimed. However, to analyse the R_a effects similar wetting characteristics (SiO_2-Al_2O_3 coated) of surface has considered for study. All the textured surfaces, namely CS3-5, CS3-10, CS3-15, and CS3-20, are inherently hydrophobic and exhibit different roughness (R_a) values as discussed in chapter 3 in details. Bubble formation on all these surfaces has been captured, and snapshots of all four surfaces under three different heat flux conditions are shown in Fig. 6.4. As the average surface roughness increases, the number of active nucleation sites also increases (from left to right in the first row of Fig. 6.4).

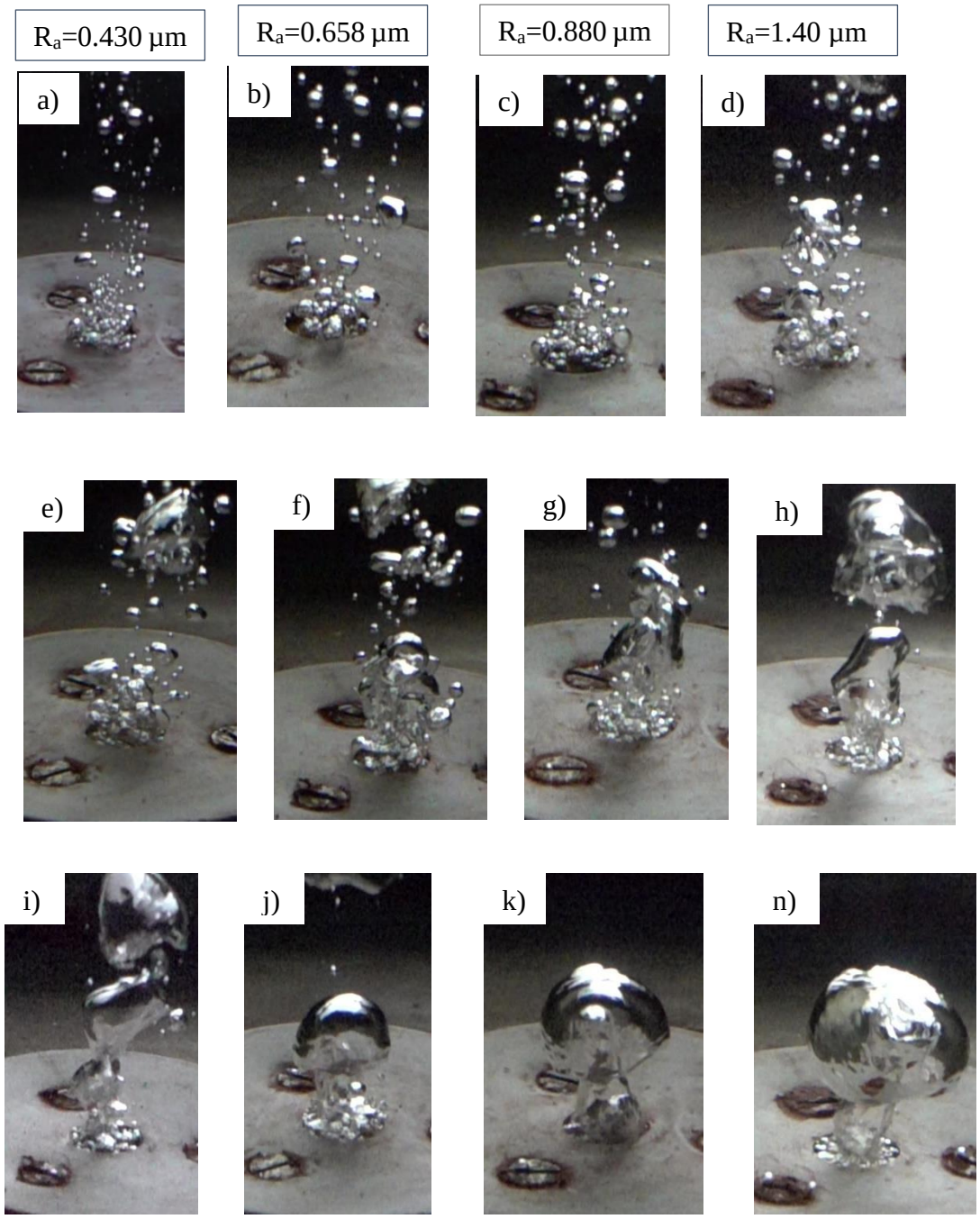

Fig. 6.4. Effects of roughness on bubble formation and their behaviour at three different heat flux condition, ((a, b, c, d) at heat flux ~55 kW/m^2, (e, f, g, h) at heat flux ~145 kW/m^2, and (I, j, k, & n) at heat flux ~310 kW/m^2).

When the heat flux increases to approximately 145 kW/m^2 the shape of the bubbles enlarges on surfaces CS3-5, CS3-10, and CS3-15, whereas on CS3-20, they begin to coalesce even before departure.

As the heat flux further increased to ~310 kW/m^2 bubbles started coalescing on all the surfaces and surfaces fully covered with the bubbles and merged with the surrounding bubble before the departure as shown in Fig 6.4(j, k, & n). In nucleate boiling region, bubble size increases, as the average surface roughness increases.

6.4. Bubble dynamics

Bubble dynamics characteristics mainly include the bubble growth rate, active nucleation site density, departure diameter, and bubble departure frequency. Bubble dynamics characteristics depends on many parameters such as surface wettability, surface texture, and surface topography. The detailed analysis of the bubble growth mechanism considering all parameters is very complex because it occurs on a very small length and time scale at the interface of the liquid and heating surface.

The mechanism of bubble growth can vary between the partial nucleate boiling region (where bubbles are isolated) and the fully developed nucleate boiling region (where bubbles coalesce to form larger bubbles). Therefore, these regions can be analysed separately using a high-resolution, high-speed camera. However, it should be noted that in the current study, a low-resolution camera (SONY RX-100V) was utilized for qualitative analysis. This camera can record videos at a maximum of 1000fps at the lowest resolution, which makes very difficult to track and focus on a single bubble. Therefore, the study of the bubble growth mechanism was not in the scope of the present work.

6.4.1. Bubble departure diameter

Bubble departure diameter play a very crucial role in boiling heat transfer coefficient. As per Mikic and Rohsenow's [34] correlation (Eq. 6.1), heat transfer coefficient is directly proportional to the square of the bubble departure diameter.

$$HTC = 2(\pi K_f \rho_f C_{pf})^{0.5} n_a (D_d)^2 (f_b)^{0.5} \quad (6.1)$$

In the present work bubble departure diameter of all surfaces estimated with the help of Eq. 6.2, which was recently developed by Kumar et al. [133] for an isolated bubble region and hydrophilic surfaces. But in the present study it applied on hydrophobic surfaces, because all surfaces are not a superhydrophobic in nature. From Eq. 6.2, it is clear that departure diameter linked to the Jacob number (Ja =$\rho_l C_{pl} \Delta T / \rho_v h_{lv}$), liquid properties and contact angle. For a particular liquid Jacob number depends on wall superheat only, which further linked to the active nucleation sites and surface textured.

$$D_d = 0.04(\sin\theta)^{\frac{3}{2}} Ja^C \sqrt{\frac{3\sigma \sin\theta}{g(\rho_l - \rho_v)}} \tag{6.2}$$

Where, C =$(\sin\theta)^{1.25}$ and θ is static contact angles

Bubble departure diameter estimated using Eq. 6.2 has plotted against Ja and shown in Figs. 6.5-6.7. If compare with the qualitative results the model predicts correct trend of D_d for textured surfaces CS2, and CS3, while for CS1 not match with the qualitative result.

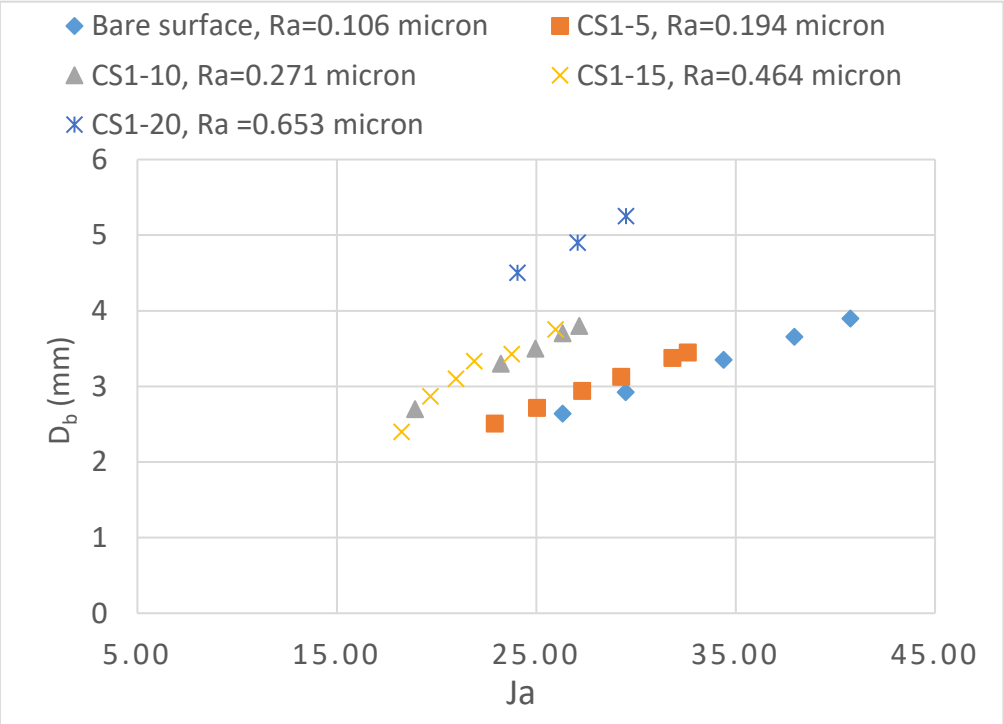

Fig. 6.5. Bubble departure diameter as function of Jacob Number (Ja) for TiO_2 -SiO_2 textured surfaces.

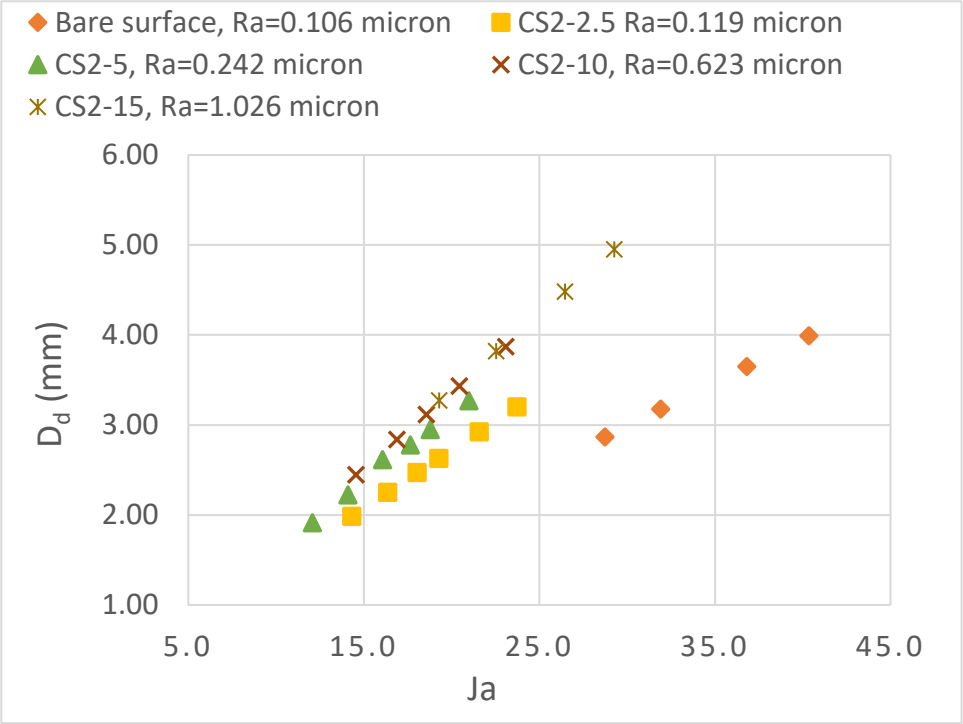

Fig. 6.6. Bubble departure diameter as function of Jacob Number (Ja) for TiO_2 –Al_2O_3 textured surfaces.

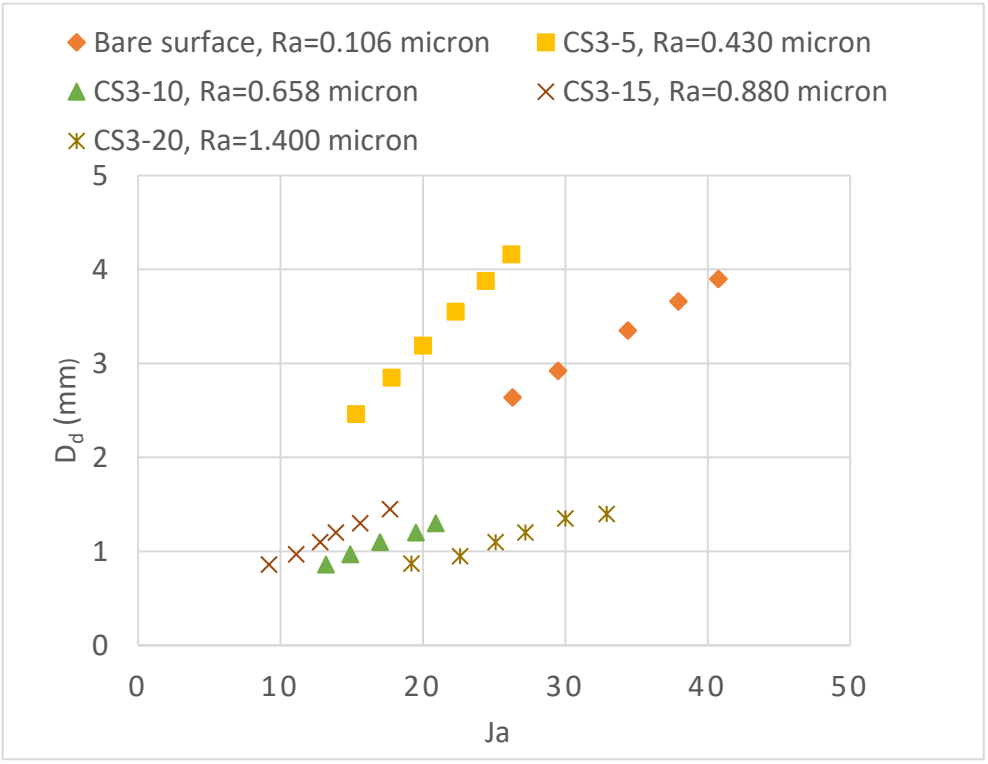

Fig. 6.7. Plot of bubble departure diameter against the Jacob Number (Ja) for SiO_2 –Al_2O_3 textured surfaces.

6.4.2. Bubble departure frequency

Bubble departure frequency also influence the heat transfer performance in nucleate boiling region. In Reference to Mikic and Rohsenow's [34] correlation (Eq. 6.1), heat transfer coefficient is directly proportional to the square root of the bubble departure frequency. Comparison to bubble departure diameter, effect of departure frequency on HTC is considerably less. Departure frequency can be calculated either experimentally or using the correlations given by various researchers. Bubble departure frequency basically defined as the inverse of time consumed in completing one ebullition cycle. The bubble ebullition cycle includes the bubble growth time (t_g) and waiting time (t_w). Growth time is the time interval between the bubble nucleation while waiting time is the time period after the departure and appearance of next bubble on same nucleation sites. If Growth time (t_g) and waiting time (t_w) known for a particular case then departure frequency (*f*) can be calculated by Eq. 6.3.

$$f\ (Hz) = \frac{1}{(t_g + t_w)} \tag{6.3}$$

It has already stated that analysis of bubble growth is not in the scope of present work due to limitation of camera used for bubble visualization which has very low resolution and identification and follow up of a single bubble is very difficult. Therefore, bubble departure frequency has estimated using well known Zuber's expression [134] (Eq.6.4), which is linked with the departure diameter as follows. Value of departure diameter calculated from Eq. 6.2.

$$fD_d = 0.59 \left[\frac{\sigma(\rho_l - \rho_v)g}{{\rho_l}^2}\right]^{0.25} \tag{6.4}$$

Figures 6.8, 6.9 and 6.10, presents the bubble departure frequency of composite textured of TiO_2 -SiO_2, TiO_2 –Al_2O_3, and SiO_2 –Al_2O_3, respectively.

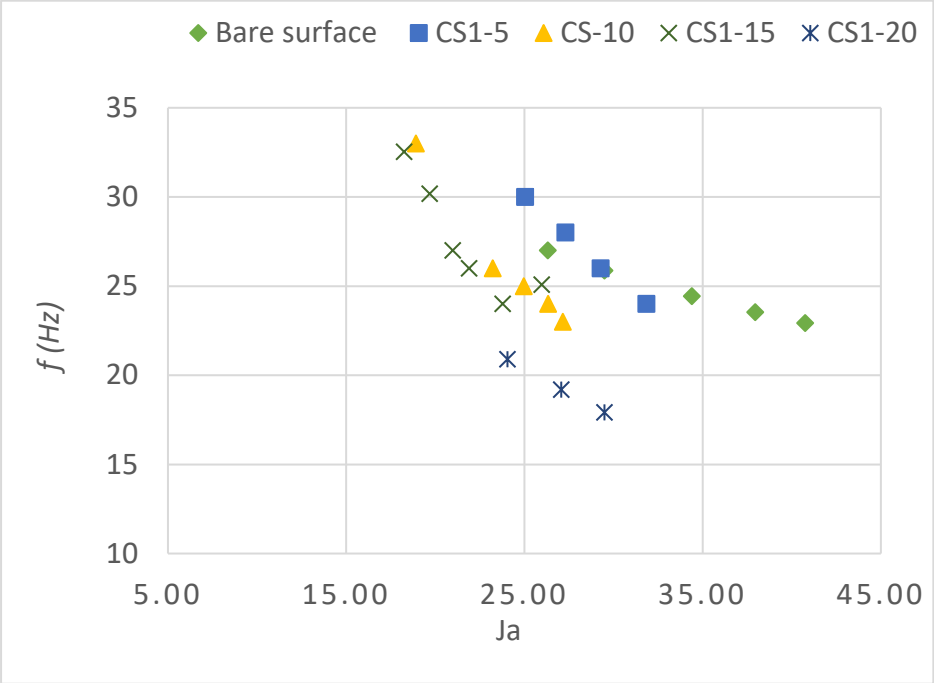

Fig. 6.8. Variation of bubble departure frequency against the Jacob Number (Ja) on TiO_2 – SiO_2 textured surfaces.

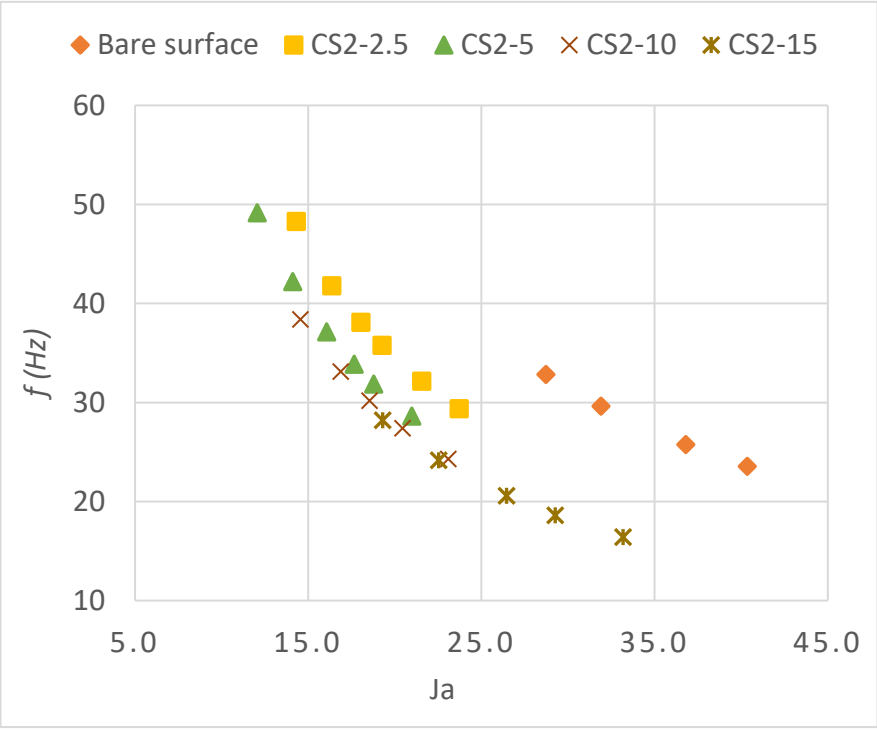

Fig. 6.9. Variation of bubble departure frequency on TiO_2 –Al_2O_3 textured surfaces.

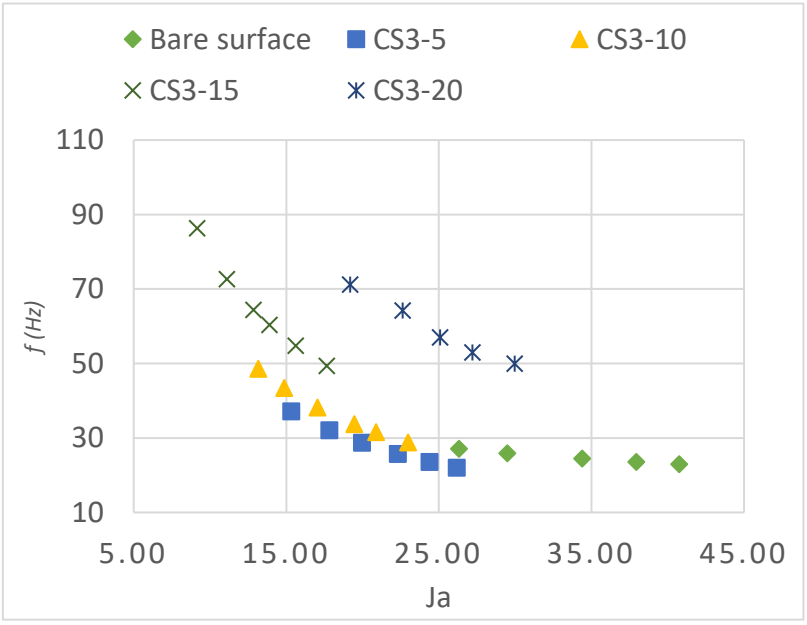

Fig. 6.10. Variation of bubble departure frequency at different Jacob Number (Ja) on SiO_2 – Al_2O_3 composite textured surfaces.

Upon carefully examination of Figs. 6.8-6.10, it can be easily noticed that the departure frequency decreases as the Jacob number (Ja) increases. The Jacob number is associated with wall superheat, and consequently, the departure frequency is also linked to the wall superheat and adversely affected by it. Because, as wall superheat increases bubble diameter also increase, resultant departure frequency will decrease (Refer Eq. 6.4). Kim et al. [135] have reported that the average roughness (R_a) also influences the bubble departure frequency on hydrophobic surfaces in the nucleate boiling regime. As surface roughness increases, the bubble size increases for a similar wall superheat, resulting a decrease in departure frequency realized as depicted in Figs. 6.8 and 6.9.

Most of the correlation or models for departure diameter has developed for the isolated bubble region and validated on hydrophilic surfaces. In present study all textured surfaces are hydrophobic in nature where bubbles start at low wall superheat and coalesce early, due to which the Kumar et al. [133] model may not predict correctly at higher Jacob number unlike hydrophilic surface.

6.5. Summary

Bubble visualization of polished copper and hydrophobic coated surface has performed at different heat flux nearly saturation temperature and atmospheric pressure condition. Bubble nucleation, bubble size, and shape analysed through snapshot of video captured by camera (Sony RX-100V) on hydrophobic and hydrophilic (bare) surfaces. Bubble departure diameter and frequency estimated with the help of semi-analytical models.

****